Powder Technology 413 (2023) 117997

Contents lists available at ScienceDirect

Powder Technology

journal homepage: www.journals.elsevier.com/powder-technology

An investigation of the effect of powder flowability on the powder spreading in additive manufacturing

Mozhdeh Mehrabi [a], Jabbar Gardy [a], Fatemeh A. Talebi [a], Amin Farshchi [a,b], Ali Hassanpour [a,*], Andrew E. Bayly [a]

[a] School of Chemical and Process Engineering, University of Leeds, Leeds LS2 9JT, UK
[b] School of Health and Life Sciences, Teesside University, Middlesbrough TS1 3BX, UK

HIGHLIGHTS

- Flowability of two grades of Ti6Al4V powder was characterised using a range of techniques.
- The powder spreading behaviour was characterised using an in-house spreading rig.
- Caution is needed when correlating powder flow behaviour with the spreadability.
- The powder flow behaviour obtained in current study cannot predict the dynamic behaviour of spreading.

GRAPHICAL ABSTRACT

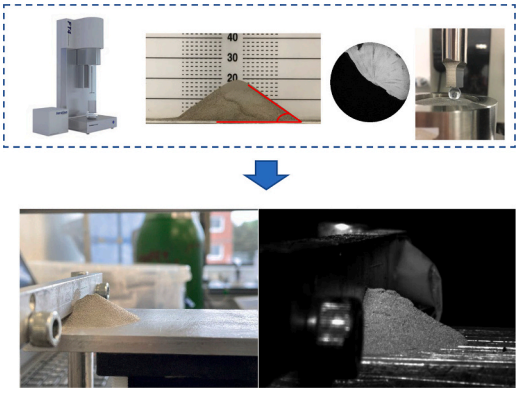

ARTICLE INFO

Keywords:
Powder bed fusion
Powder spreading
Powder flowability
Ball indentation
Ti6Al4V powders

ABSTRACT

Identification of the most reliable method to characterise powder flow behaviour in correlation with the conditions of powder spreading in additive manufacturing (AM) is still challenging. In this study, a number of standard and advanced flowability techniques were used to characterise the flowability of two grades of Ti6Al4V powder (gas atomized, GA, and hydride-dehydride, HDH) used for the powder bed fusion (PBF) based AM. In parallel, the powder spreading behaviour was characterised using an in-house spreading rig. It is found that GA powder has better spreading behaviour than HDH, owing to its better flowability due to the regular particle shapes. However, none of the flow test techniques investigated in this paper can offer a correlation between the dynamic powder flow and powder spreadability at varying speeds. The study in this work has revealed the shortcomings in correlating the flowability of powder and their spreadability under real process conditions.

* Corresponding author.
E-mail address: A.Hassanpour@leeds.ac.uk (A. Hassanpour).

https://doi.org/10.1016/j.powtec.2022.117997
Received 5 July 2022; Received in revised form 30 September 2022; Accepted 5 October 2022
Available online 11 October 2022

1. Introduction

Additive manufacturing (AM) is a novel production technique which has received a significant amount of industrial attention due to its advanced technical innovation which has resulted in, for example, less labour work to produce unique and complex-shaped metal parts [1]. The current additive manufacturing applications are categorised into two main classes, i.e., powder-bed based, and powder-fed systems. Powder bed-based fusion system (PBF) is also divided into the selective laser sintering (SLS) for polymeric material and selective laser melting (SLM) and electron beam melting (EBM) for metals [2–4].

The PBF technology has lately been considered as a desirable production route of dense components with improved performance such as structural complexity, thermal behaviour and required mechanical properties [4]. The PBF techniques consist of powder a hopper (or reservoir), blade, build plate and a heat source (Fig. 1). First the powder is spread by a blade where a thin layer of powder can be created with a thickness between 20 and 200 μm (depending on the process condition), then an energy source (beam, laser) selectively melts the area layer by layer according to the 3D CAD file of component [5–7].

Nowadays, the EBM process is one of the widely used techniques to fabricate Ti6Al4V components for biomedical, aerospace and automotive applications for its excellent properties such as: 1) high toughness; 2) good corrosion and creep resistance; 3) relatively low elastic constant (roughly around 110 MPa compared to Stainless steel with a Young's modulus of 200 MPa) [8]; 4) high ratio of strength to weight which is the main reason to be used in aerospace and biomedical industries [9]. There are different powder manufacturing techniques to produce Ti6Al4V alloy from various vendors. Gas atomization (GA), hydration-dehydration atomization (HDH), plasma rotating electrode process (PREP) and plasma atomization (PA) are the primary methods to produce titanium powder for SLM and EBM [10,11]. Based on different manufacturing techniques, powders can have different characteristics such as shape, size and surface properties which can consequently influence the bulk powder characteristics, e.g. the powder bed spreadability and hence the built part properties such as strength and corrosion resistance. Powder spreading plays a key role in the PBF process; the more uniform the powder spread layer, the higher the particle packing density [12]. However, in general there is still insufficient understanding of correlation between the powder flow and spreading in additive manufacturing using the PBF systems [13,14].

A comprehensive understanding of the relationship between particle properties and the built component's performance is of significant importance in additive manufacturing (Fig. 2). However, there is no general agreement in the literature regarding the effects of powder properties on the final product such that different authors may suggest contradictory statements. For instance, regarding powder size as a powder property, Shi et al. [16] and Simchi et al. [17] state that finer particles have a negative impact on the layer density as they are susceptible to agglomeration. On the other hand, some researchers favour the use of fine particles as they improve the surface roughness due to efficient packing [18–23]. Morphology is another important powder property that needs to be precisely measured since it directly impacts the performance of the end product. Majority of authors agree that spherical particles are desirable in additive manufacturing as they increase the homogeneity of layers, which decreases the surface roughness and increases the volume fraction [12,24]. Additionally, spherical and smooth particles are thought to be beneficial for the end product as they aid in creating compacted layers with lower surface roughness presumably due to their enhanced flowability [24–28]. Generally, there is a direct correlation between the sphericity of Ti6Al4V powders and their production cost [2], therefore, there is a general desire to utilise powders manufactured by lower costs, e.g. the hydrate-dehydrate processes (non-spherical). However, majority of recent studies are focused on spherical Ti6Al4V powders which are usually manufactured by gas or plasma. Overall irregular powders have worse flowability than the spherical powders, but flowability is a complex behaviour that cannot be simply characterised by only using single flowability measurement technique for the AM process, since there is no specific method established to simulate the motion of bulk power under the spreading process [29–31]. Owing to the significance of powder bulk characterisation for additive manufacturing, here we provide a brief review of previously used characterisation techniques for AM powders, with a specific focus on different grades of Ti6Al4V powders.

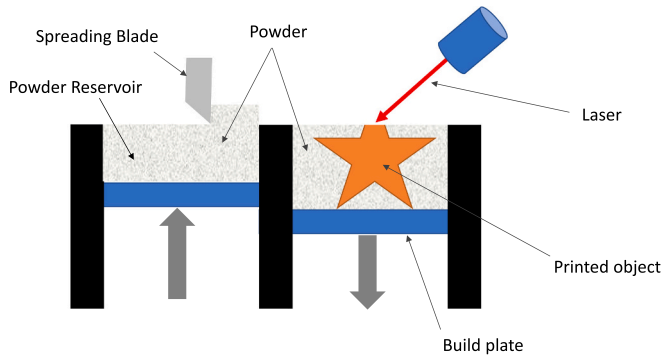

Fig. 1. The schematic of PBF mechanism.

2. Flowability measurements techniques

There are number of techniques that are universally used in powder industries. Some of these methods are used more frequently in AM which are discussed below.

2.1. Tapped density

The method introduced by (Hausner 1967) is one of the most commonly used measurement techniques to characterise powder flowability [32]. It is the ratio of the tapped density (mass per volume after mechanically tapped) over the apparent density (mass per volume of free fall) powder. The change in volume and ability of powder to move after tapping is related to inter particle friction and cohesion which has direct impression of powder flowability. Carr index [33] is the ratio of the difference between the tapped and bulk densities to tapped density. Essentially the lower Hausner ratio (HR) and Carr index (CI) indicate that the powder is more free flowing and less cohesive. There are few research work suggesting that HR could be an indicator of flowability for the AM powders [23,34].

2.2. Angle of repose (AOR)

The angle of repose is a simple method for measuring powder flow [35]. In this test, the powder is poured freely through the specific funnel size to make a pile settled under gravity. The slope angle of the conical pile of powder to the free surface (horizontal base) is the angle of repose and is considered as a measure for powder flowability, although the measurements could be somewhat user dependent [36]. Due to the simple sample preparation and quick performance, this technique is usually used for quality control and comparison of different bulk powders.

However, Sun et al. [29] concluded that this technique is not useful to characterise flowability and could not link the AOR to the process performance of powders in AM. It is worth noting that the test conditions, could be considered close to the stage of powder feeding and heap formation during the AM process.

2.3. Dynamic angle of repose (Avalanche angle)

This technique typically consists of a rotating, transparent drum

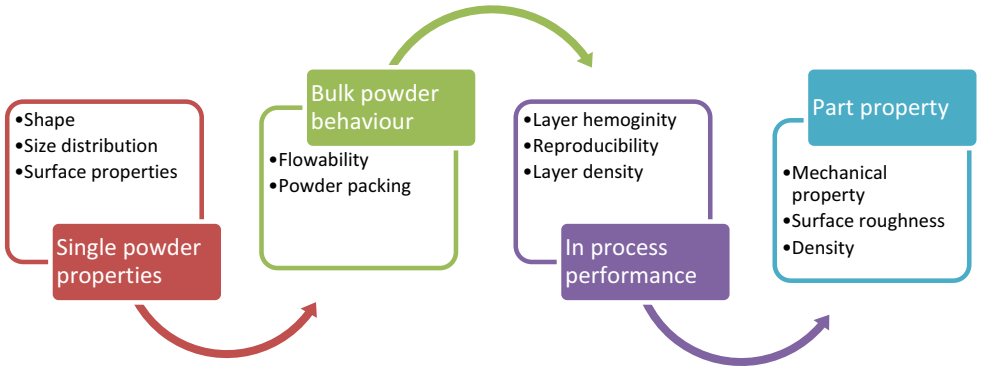

Fig. 2. Influencing parameters and their analysing method on metal powder for AM process [15].

filled with a certain amount of powder and a camera in front of a backlight. The camera records pictures of the powder free surface and the cross-sectional area of powder inside the drum during rotation. The pictures can be analysed for powder avalanche angle and surface fractal, which are associated with powder flowability and inter particle forces [37]. Gu et al. [38] used this method to characterise flowability of three different Ti6Al4V atomized powders from different suppliers (EOS GmbH, LPW Inc. and Raymor Industries Inc.) and found a direct correlation between the powder flow characteristics and part properties after the SLM process.

2.4. FT4 Rheometer

The FT4 Powder Rheometer, developed by Freeman Technology (Tewkesbury, UK), can be used to characterize the powders in motion. Flow properties such as flow energy and bulk density could be measured in dynamic regimes [39]. The standard test procedure allows two types of powder flow pattern to be examined. The vessel is filled with the powder and the impeller is initially rotated clockwise through the vessel to measure powder flow under a relatively confined condition. Following this, flow properties can be determined by rotating the blade anti-clockwise and moving it upward where the powder flow could be determined under an unconfined condition (Fig. 3).

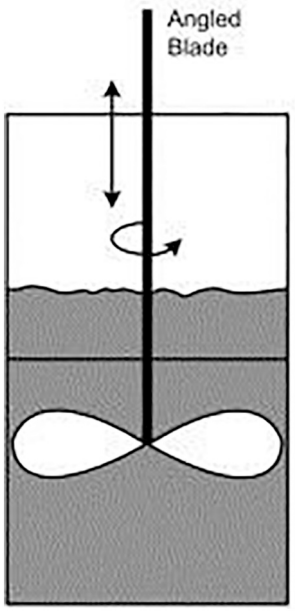

Fig. 3. Dynamic powder testing determines the flowability of a powder from measurements of the axial and rotational forces acting on a rotating blade.

The specific flow energy is the work that is done to move the powder by moving the blade upward and because the powder is unconfined, the energy calculated is mostly dependent on the inter-particle forces [39,40]. Clayton reported the measurement of dynamic flow properties of virgin, blended, and used GA Ti6Al4V powders by using the FT4 and concluded that this method is very helpful in optimising lifecycle management right through from virgin powder to final waste. Their assumption was based on the fact that the used powder would not flow as freely as the virgin material, hence it is consequently less likely to successfully perform in the process [40]. Recently Narra et al. investigated the use of Ti6Al4V HDH powder for the EBM process which showed spreading defects as opposed to atomised powders. This difference was correlated with the specific energy of HDH and atomised powders obtained from FT4 rheometer. A modification to the opening of spreading hopper has eventually led to the successful use of non-spherical HDH powder in the EBM process [41], presumably due to a more consistent/better flow out of the hopper.

2.5. Powder flowrate

Powder flowrate or Hall flowrate is the most frequently used method to measure flowability for free flow powders and is widely used for metal powders. The time required to discharge a certain amount of bulk powder through a calibrated orifice size can be used to measure flowability of powder. This method is very cheap and simple and can be widely used for AM powders [42]. However, Schulze [43] defined some drawback of this method such as operator dependency (type of filling) and the effect of aeration of the powder on flowrate. From this he concludes that funnel tests are only simple comparative tests not allowing a quantitative statement on powder flow [43]. Although the test conditions could be similar to the gravity assisted powder discharge out of the spreading hopper, Sun et al. stated that this method solely, cannot distinguish the differences between the titanium powders with the concern of their behaviour in EBM process [29].

2.6. Ring shear cell

Shear cell is well known measurement technique to determine flowability at moderate or high stress condition with good reproducibility [40]. This method gives a good insight into powder properties such as powder flowability, compressive strength, powder compressibility, consolidation time “caking”, internal and wall friction, and bulk density [43]. Despite of its wide usage in academia, shear cell could not be a useful technique for measuring powder flow at high shear rate which resembles the AM process conditions during the spreading stage. Tan et al. has evaluated the powder flowability of twelve AM powders including atomized and milled Ti6Al4V powders based on the principal component analysis of different test results including shear cell. They concluded that flow factor from shear cell results has the lowest weight

on correlation between flowability and spreading process [44].

2.7. Ball indentation

Ball indentation on powders has been introduced by Hassanpour and Ghadiri [45] to characterise powder flow behaviour. The indentation technique gives a measurement of resistance to plastic deformation under the specific force (Fig. 4).

Through the process the applied load (F) and penetration depth (h) are recorded for both loading and unloading cycles as shown in Fig. 5. The indentation will result in an imprint with a projected area, A:

$$A = \pi\left(d_b h_c - {h_c}^2\right) \tag{1}$$

where d_b is the diameter of the indenter and h_c is plastic depth which is determined by the intercept of the tangent to the unloading curve.

The indentation hardness (H) of bulk powder bed which is resistive pressure at the tip of the indenter can be determined by Eq. (2):

$$H = \frac{F_{max}}{A} \tag{2}$$

where F_{max} is the maximum applied load and A is projected area of the impression.

However, for bulk solid of powders, during the plastic deformation under load of indenter, the material around the indenter can deform elastically and cannot flow easily which causes the increase in local flowing stress. This may cause the hardness of powder become greater than the plastic yield stress. The their ratio between the two stresses is called the constraint factor Eq. (3):

$$C = \frac{H}{Y} \tag{3}$$

where C is constraint factor, H is hardness and Y is yield stress.

This technique allows flow measurements at low stress levels which is closer to the AM process condition but has not been yet evaluated for the powders in additive manufacturing.

The above review revealed that there has been numerous works on the powder characteristics of Ti6Al4V powders but there is lack of a systematic comparison between powder flow characteristics of GA and HDH Ti6Al4V powders, especially with reference to the spreading behaviour of the two grades which is the important step before sintering in AM. Therefore, in this paper we investigate and compare the flowability of two grades of Ti6Al4V powders, obtained by gas atomized (GA) and hydration-dehydration (HDH) processes, using a range of powder flowability characterisation techniques such as density measurement, static and dynamic angle of repose, FT4 rheometer, ring shear cell, ball indentation and powder flow rate through and orifice. The powder spreading performance is then evaluated using an in-house spreading apparatus to reveal possible correlation with a specific flowability technique(s).

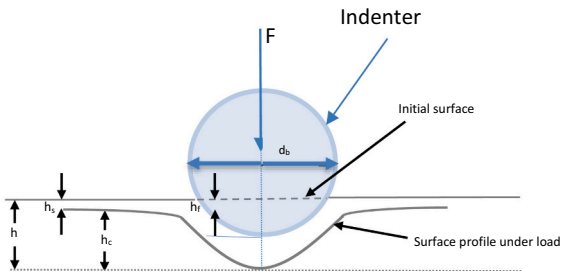

Fig. 4. Definition of variables for hardness calculation.

3. Material for experiments

In this work two grades of Ti6Al4V powder obtained from different manufacturing processes have been investigated: (i) HDH, with irregular shape particles (Fig. 6a) and (ii) GA, with nearly spherical particles (Fig. 6b).

The equivalent diameter, sphericity and aspect ratio of both samples were previously measured by X-ray microtomography (XMT) technique, as this can give additional information about their flowability [31]. Close up XMT images of GA and HDH particles are also presented in Fig. 7a, b.

The particle size distributions of both powders were previously measured [31] by laser diffraction technique (dry method) using the Mastersizer 3000 Particle Size Analyzer (Malvern analytical, UK) and their shape characteristics of were analysed by G3 morphologi (Malvern analytical, UK). The results are summarised in Table 1.

4. Results and discussion

4.1. Density and compressibility

100 g from each powder was used for the density measurements, using the Copley JV 2000 tapped density tester (Copley Sci., UK). During the measurements, the lab ambient conditions were relatively stable around 40% relative humidity (RH) and 22 °C. Also, the Pycnomatic ATC (Thermo Scientific™) system was used to measure the true density of the powders according to the ASTM B923 standard. Table 2 shows the result of the powder true density, bulk and tapped densities, HR, and CI. It can be seen that both samples have close true densities, but GA has higher bulk and tapped density with lower HR and CI, indicating to a better flow than HDH powder.

4.2. Angle of repose

The Powder Research Ltd. AOR Tester was used to measure the angle of free surface of discharged powder to the horizontal plane. 50.0 g from each powder was used for the tests, under the lab ambient conditions (40% RH and 22 °C). The illustration of angle of repose for both samples are presented in Fig. 8. It can be seen that HDH powder slightly scatters and sticks to the wall during the experiments.

As shown in Table 3, the average results of AOR for GA was 27.1° while HDH had the AOR of 37.6°. Both samples show good flowability, however GA has a smaller angle of repose and therefore a better flowability as compared to HDH.

4.3. Dynamic angle of repose (Avalanche angle)

The GranuDrum supplied by Granutools™ was used for the Dynamic angle of repose measurement. The system consists of a glass sided drum which was loaded with 100 g from each powder and rotated at 2,4,6,8 and 10 rpm while a charged coupled device CCD camera collected snapshots and data for each rotating speed. Based on GranuDrum powder tester guidelines these rpms would result in a slumping regime for the powder flow. The avalanche angle is the angle of powder surface just before the avalanche starts.

Fig. 9 presents the illustration of both powders just before and after the first avalanche at 2 rpm. Each powder was tested three times at each rpm and the average avalanche angle was calculated as 33.4° and 46.5° for GA and HDH powders, respectively. It was observed that HDH powder formed higher surface fractal as a result of inter-particle forces presumably due to particle shape and surface roughness. Similar to the angle of repose test, the HDH powder scatters and sticks to the equipment wall as seen in Fig. 8.

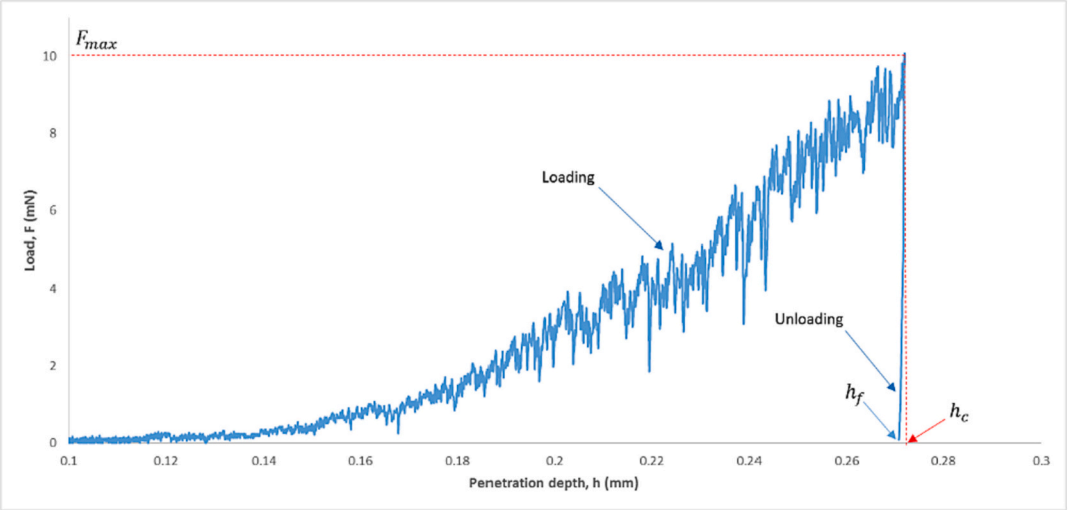

Fig. 5. Schematic curve of penetration depth against load for Powder GA (loading-unloading curves).

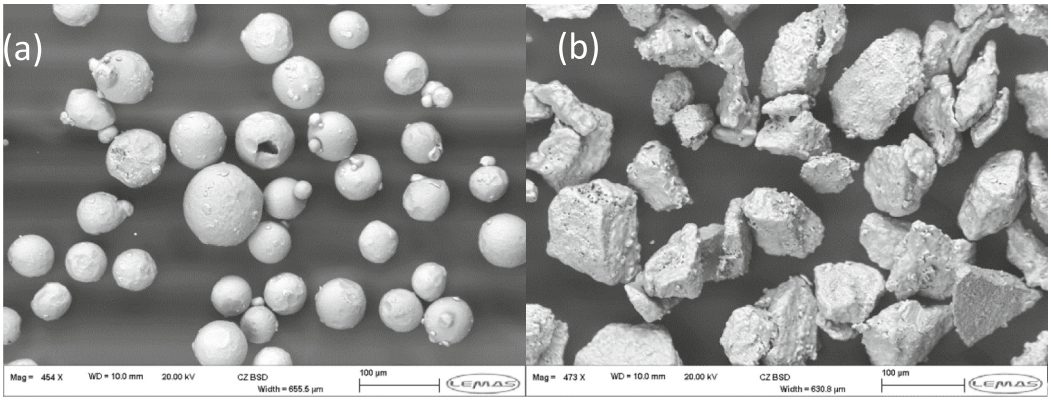

Fig. 6. SEM images of (a) gas atomization (GA) and (b) hydration dehydration atomization (HDH) of Ti6Al4V samples.

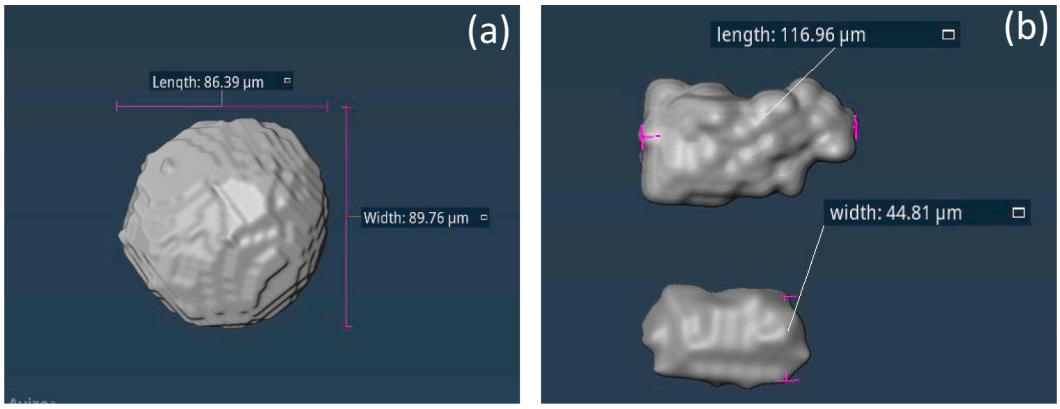

Fig. 7. Close up images of XMT reconstructed particles (a) GA and (b) HDH [31] at 7-µm pixel size.

Table 1
Size and shape quantiles of both samples based on Mastersizer and G3 Malvern.

Powder	D_{10} (µ)	D_{50} (µ)	D_{90} (µ)	Aspect ratio	Sphericity
Ti6Al4V (GA)	48	70	102	0.9	0.96
Ti6Al4V (HDH)	63	100	158	0.7	0.77

4.4. FT4 Rheometer

Freeman FT4 powder rheometer has been used to determine powder flowability in a dynamic regime. Results are presented in Fig. 10 which show a sequence of 11 flow tests for both samples. The first seven tests were performed at 100 mm/s tip speed of rotating blade, followed by the remaining 4 tests at variable blade tip speeds (test number 8–11 at 100, 70, 40 and 10 mm/s, respectively).

Table 2
Scale of flowability related to tapped density for both samples.

Materials	True density (g/ml)	Bulk density (g/ml)	Tapped density (g/ml)	Hausner ratio (HR)	Compressibility index (CI) %	Scale of flowability
GA	4.44	2.6	2.8	1.07	6.2	Excellent
HDH	4.47	1.9	2.1	1.10	9.5	Good

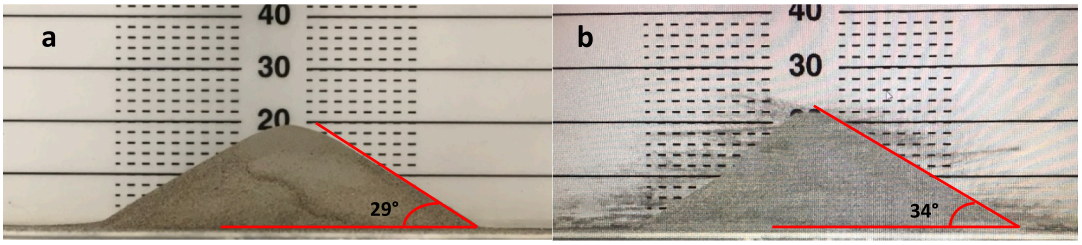

Fig. 8. Experimental set up of AOR on (a) GA and (b) HDH samples.

Table 3
Angle of repose results for both samples.

Angle of repose		Scale of flowability
GA	27.1 ± 0.1	Excellent
HDH	37.6 ± 0.1	Good

The dynamic testing of the samples was performed with three replicates. The mean values of the measured parameters are presented in a Table 4.

The Basic flow energy (BFE) which is the energy required to displace the powder during downward movement of the blade, is found to be 260.0 and 249.0 mJ for GA and HDH powders, respectively. However, HDH powder has a higher ratio of BEF per unit of mass (Normalized Basic Flowability Energy (NBFE)) than GA. The specific energy (SE, the energy required to displace the powder during the upward movement) indicates how the powder will flow under an unconfined state. The higher values of SE for HDH powder indicates that it has a lower flowability due to the irregular particle shape and particle interlocking. The conditioned bulk density (CBD) corresponds to the density of a sample inside the vessel of FT4 after the pre-conditioning step. The results show that the HDH powder demonstrates poor packing behaviour as compared to GA powder. The CBD measured by FT4 has been found to be lower than that of tapped density due to the different conditions of samples in the FT4 vessel. Interestingly, an increase in flow energy level is observed for both GA and HDH powder with reducing the blade tips speed (70, 40 and 10 mm/s) compared with those measured in constant flow rate zone, which indicates to the dependency of powder flow to the dynamic conditions. Comparing the flow rate index (FRI), HDH powder has shown a little more sensitivity to the blade tip speed than GA powder.

4.5. Powder flowrate

Powder flow rate through an orifice was investigated using the GranuFlow apparatus (Granutools ™). The plot of "mass flow rate"

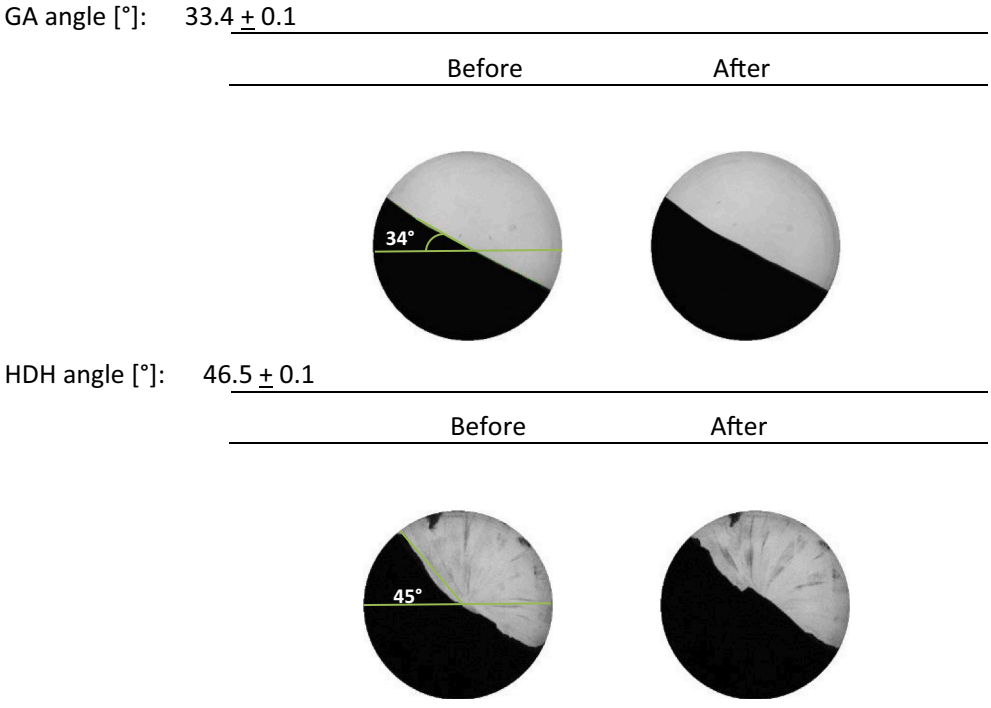

Fig. 9. Illustration of surface fractal and avalanche angle for top (GA) and bottom (HDH) powders just before and after avalanche happening.

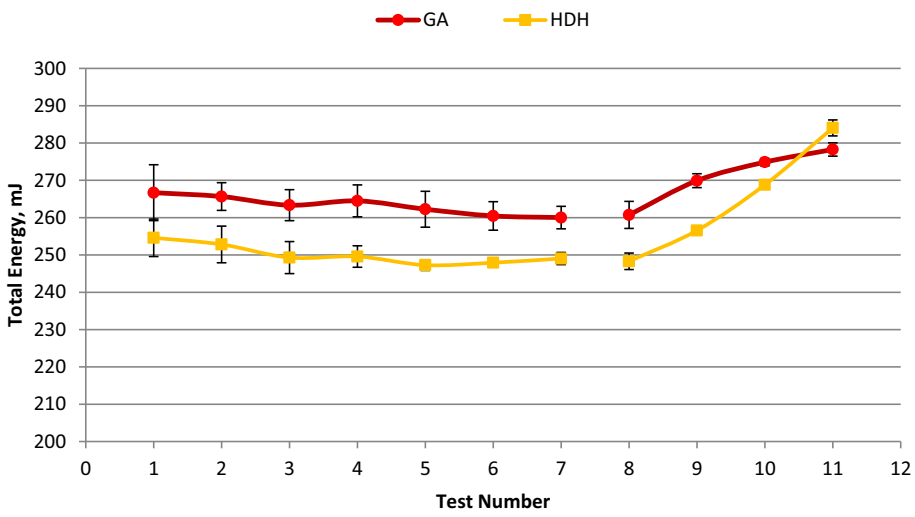

Fig. 10. Flow energy measurement at fixed and variable blade tip speed.

Table 4
Parameters used to describe flow behaviour, derived from FT4 rheometer.

	BFE (mJ)	NBFE	SI	FRI	SE (mJ/g)	CBD (g/ml)
GA	260.0	4.07	0.98	1.07	2.34	2.06
HDH	249.0	5.28	0.98	1.14	3.05	1.40

versus aperture size is presented in Fig. 11.

It can be seen that the mass flow rate for the GA powder is higher than the HDH powder for all the tested aperture sizes.

To evaluate the powder flow rate through smaller orifice sizes, an in-house powder flowmeter equipped with a variable iris aperture was developed at the University of Leeds (Fig. 12a). 30 g from each powder was gently poured into the hopper while the orifice on the bottom was completely closed, then it was slowly opened until the powder started to flow. The smallest orifice that enabled the powder flow can be identified in this way, which is commonly known as "flow index" [47]. Fig. 12b and c shows that both powders have the same flow index (1 mm), however, HDH exhibits a behaviour similar to the rat-holing phenomenon, which occurs when discharge of powders takes place only in a flow channel located above the outlet and all powder flow from other part of hopper stops.

4.6. Ring shear cell

The standard flow measurements was performed using the Schulze Ring Shear Cell RST-XS at University of Leeds. The flow properties of powders under lower consolidation stress were determined using the low consolidation RST-XS.s shear cell at University of Surrey. These tests were performed at low pre-shear stresses which are not achievable with standard shear cells, to examine the flow behaviour in a low-stress range. Metal powders have high density and their sample weight could be considerable, it is worth noting that the weight of powder is already taken into account by the controller software for the calculation of consolidation stress.

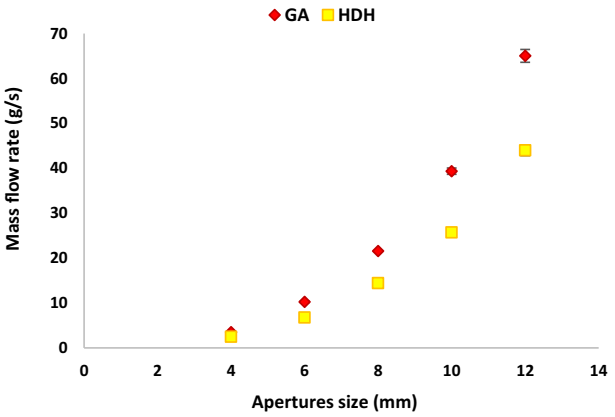

Fig. 11. Profile for GA and HDH powders.

The unconfined yield strength versus the major principal consolidation stress for both standard and low stress shear tests on both powders is presented in Fig. 13.

These results show that at high consolidation stresses (>3 kPa) GA has better flow behaviour than the HDH. However, at low consolidation stresses (<1 kPa) the HDH powder flow behaviour improves and gets closer to the GA powders. It should be noted that the minimum consolidation stress which gives reliable results for GA and HDH powders were around 426 Pa and 679 Pa, respectively.

The flow function (FFc) at 5967 Pa consolidation stress, which corresponds to the smallest major consolidation stress for HDH sample from standard shear cell, and the average internal angle of friction of both samples are presented in Table 5. The flow function at this major consolidation stress for GA powders has been found by the interpolation of data from the two available data points. The results indicate that both powders are in the free flow region, however, GA powder has better flowability than the HDH powder.

The results of low stress shear test from Table 6 indicate that at 679 Pa major consolidation stress (the smallest stress for HDH powder) the flow functions of GA and HDH powders are 14.9 and 10.7, respectively. Although still under the free flowing category, at low stress the flowability of GA powders reduces while it improves for the HDH powder. One possible reason for improving flow behaviour of HDH powder at low consolidation stress could be the irregular shape of HDH particles which could result in less interlocking at small stresses as opposed to the higher consolidation stress levels.

4.7. Ball indentation

In order to determine powder flowability at lower stresses than those achieved by the low consolidation shear cell ($\leq$ 0.5 kPa), the ball indentation technique was used to investigate the powder bed hardness of both samples using the Instron 5566 mechanical testing machine (Instron Corp. USA) at Leeds University. Fig. 14 shows the setup of ball indentation which consists of a high precision spherical glass ball

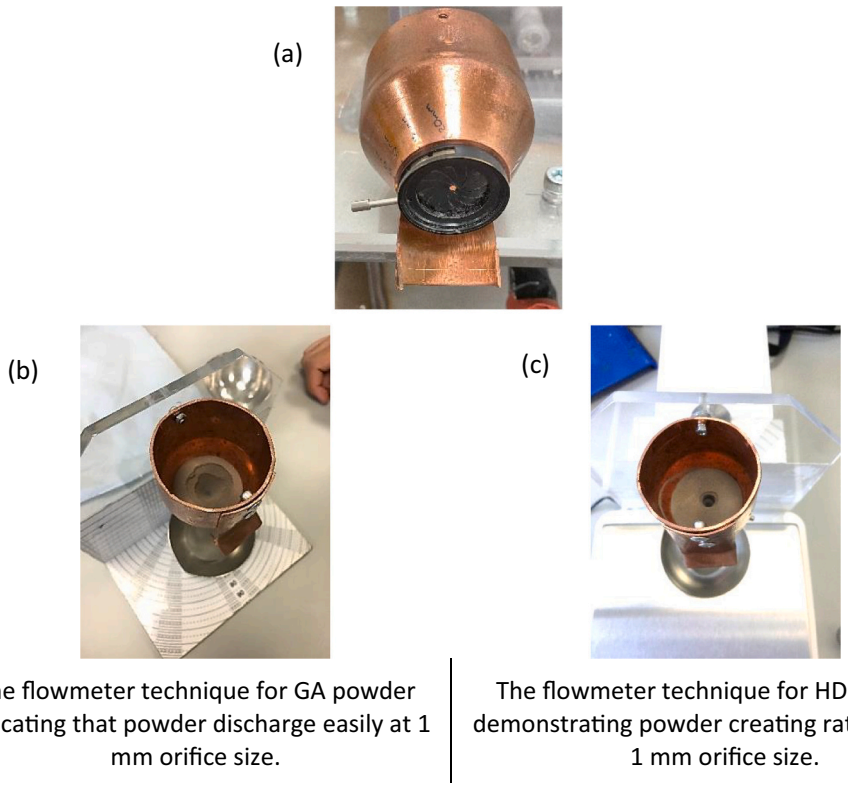

Fig. 12. The orifice outlet powder flowmeter (a) and top-down view of the flow channel formed inside the cylinder at 1 mm orifice for (b) GA powder and (c) HDH powder.

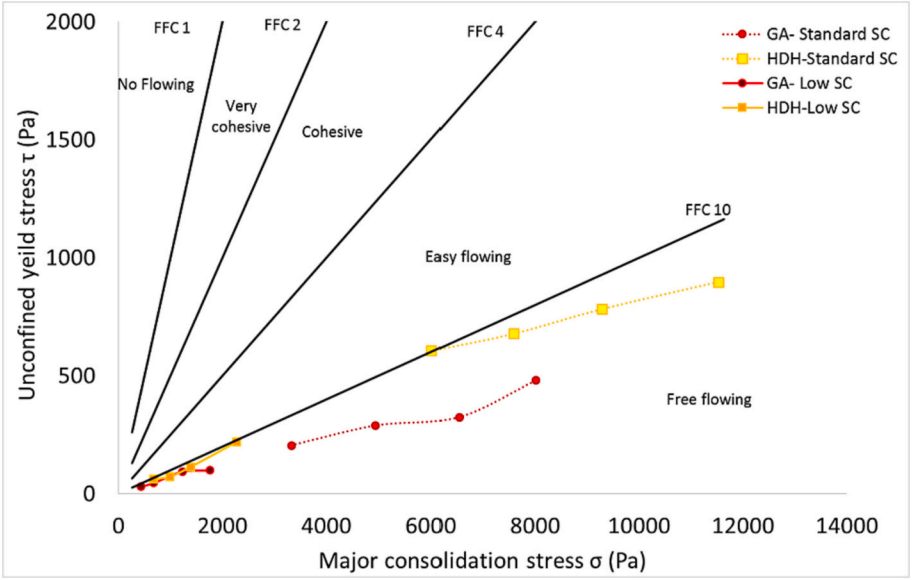

Fig. 13. Ring shear test results for both samples GA and HDH (Ti6Al4V) at standard and low shear cell (SC).

Table 5
Powder flow properties driven from standard shear cell results.

Standard shear cell	GA	HDH
Flow function at 5967 Pa	19.1	9.8
Internal angle of friction (°)	32	43

Table 6
Powder flow properties driven from low-stress shear cell results.

Low shear cell	GA	HDH
Flow function at 679 Pa	14.9	10.7
Internal angle of friction (°)	32	44

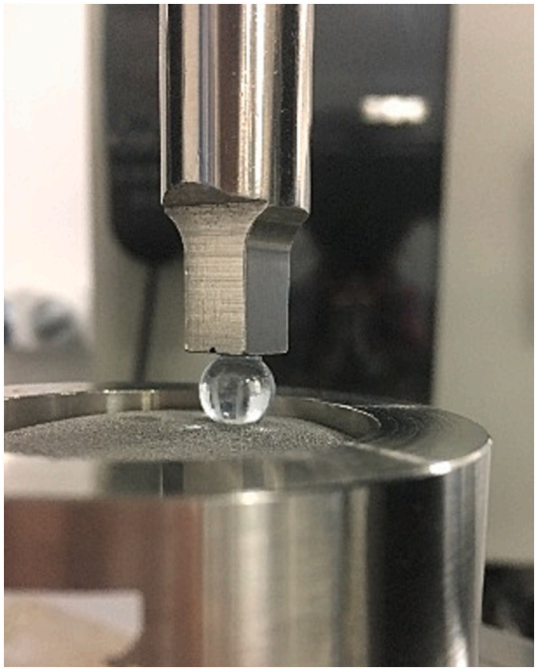

Fig. 14. Experimental set up of ball indentation.

indenters (8 mm, Sigmund Linder GmbH, type M), a stationary anvil, and the die made of stainless steel with an inner diameter of 20 mm.

According to method suggested by Zafar et al. [46] samples were fed into the die using the sieving method.

To minimize the effect of filling and history of powder the samples were first conditioned in a die by using the JV 2000 Copley Tapped Density tester (Copley Sci., UK) at 30 taps (where there was no further change in the sample height).

The first test was carried out without any consolidation (0 Pa) and an indentation hardness test was conducted at 10 mN load with a constant strain rate of 0.1 mm/min. For the rest of the tests, the powder bed was uniaxially compacted to the range of 100–5000 Pa consolidation pressures. The ball indentation test was then carried out on the compressed powder bed using 10 mN indentation loads. The tests were carried out under ambient conditions (temperature between 21 °C and 23 °C and relative humidity between 40% and 50%.

As shown in Fig. 15, the hardness of HDH powder is slightly higher than the GA sample which indicates to a lower flowability. At smaller consolidation stresses (<500 Pa) the HDH powder bed hardness gets closer to that of GA; which is a similar trend to that observed for the low stress shear cell tests.

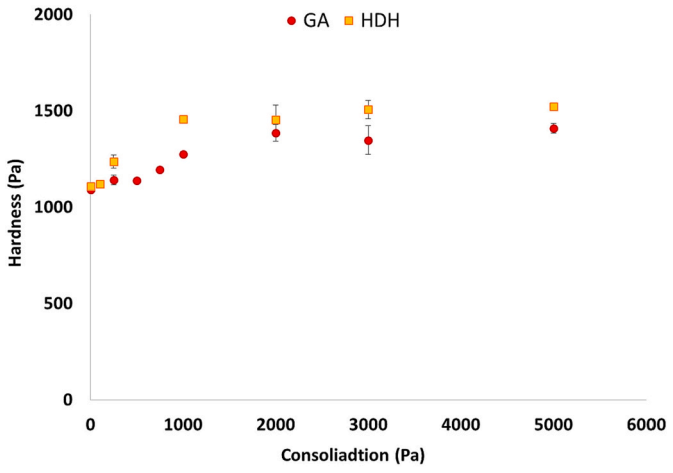

Fig. 15. Hardness measurement of GA and HDH powders at different consolidation pressures.

4.8. Summary of powder flowability techniques

The results of flowability from seven different flow measurement techniques for both powders are presented in Table 7. It can be seen that all techniques suggest that GA powder has a better flowability than the HDH powder, owing to its regular shape.

4.9. Spreadability of powders

To measure the quality of the spread powder layer, a spreading rig set-up was designed at the University of Leeds (Fig. 16 a). The rig consisted of a build plate (length: 115 mm, width: 65 mm), which can be moved to achieve different spreading velocities, and a stationary blade which is adjusted vertically to optimize a desirable gap size. In BPF systems, the powder is spread and then sintered either by a laser or an electron beam. The first layer of powder is spread then after sintering/fusion, the built plate is lowered which could create a shallow empty pocket for the subsequent powder layers to be spread. To account for this configuration, the build plate in this wok consists of a shallow a pocket (1 mm depth) as shown is Fig. 16b.

In this work, we have also considered spreading on a free surface with no confinement (Fig. 17) to assess the spreading behaviour under an unconfined condition and compare that with the spreading under a confined condition.

In this work, for both systems the powder was weighed and poured in front of the blade though a funnel to create a heap (Fig. 18) before the start of each spreading test. In this way, we could minimise the influence of powder flow rate and feeding on spreading. The gap between blade and bed was adjusted and calibrated by using a "feeler gauge" and then the plate was moved at different spreading speeds ranging from 50 to 200 mm/s. A layer of powder was spread over the plate and the excessive powder was collected at the end of plate. The density of the spread powder layer is the main factor that influences powder solidification and as a result the quality of the final part [49]. The powder bed density was calculated by using Eq. (7):

$$\rho_b = \frac{m_{powder\ bed}}{V_{Powder\ bed}} \tag{7}$$

where, ρ_b is packing bed density, $m_{powder\ bed}$ is the mass of spread layer on the powder bed and $V_{Powder\ bed}$ is the volume of powder calculated by the area of the spread and the gap size. Here we assumed that the bed height is uniform across the plate and is similar to the gap size. In future, the spreading rig could be assisted by a laser profiler to precisely measure the bed height profile across the plate.

Cordova et al. [48] suggested that relative density (RD) of spread powder (apparent density/true density) could be used to examine the

Table 7
Comparison on of different flowability tests for both samples.

	GA	HDH
Hausner ratio	1.07	1.10
Compressibility index (CI) %	6.2	9.5
Static angle of repose	27.1	37.6
Dynamic angle of repose	33	46
Internal angle of friction	32	43
Flowrate (g/s) at 12 mm aperture	65.0	44.0
Flowrate (g/s) at 4 mm aperture	3.5	2.5
SE (mJ/g)	2.02	6.28
Standard shear cell flow function at 5967 Pa	19.1	9.8
Low shear cell flow function at 679 Pa	14.9	10.7
Ball indentation hardness @ 0 Pa (Pa)	1088.9	1109.4
Ball indentation hardness @ 250 Pa (Pa)	1141.7	1235.7
Scale of flowability	**Excellent**	**Good**

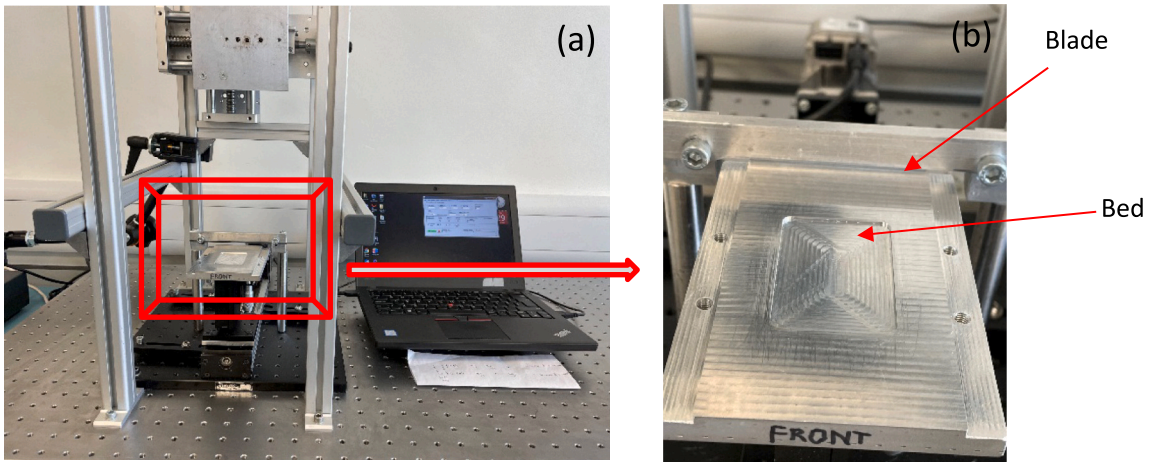

Fig. 16. (a) Rig set up of spreading process and (b) the build plate with pocket.

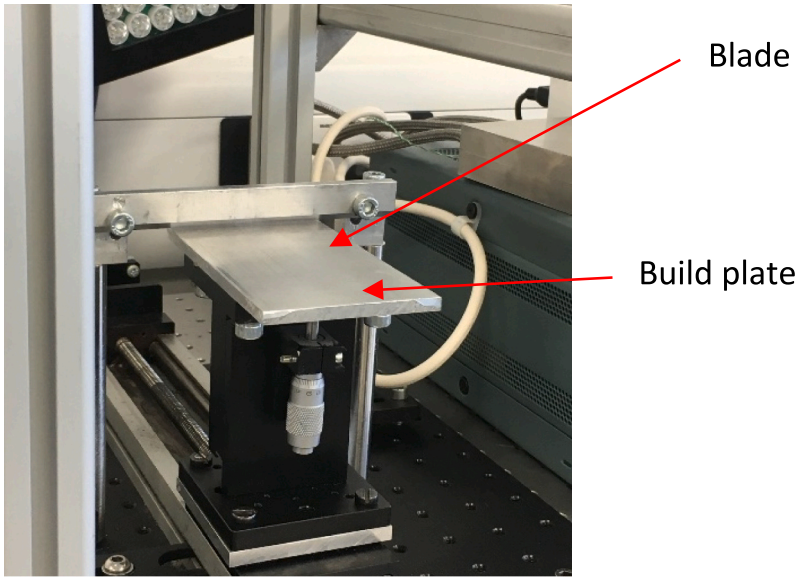

Fig. 17. Spreading on a flat build plate.

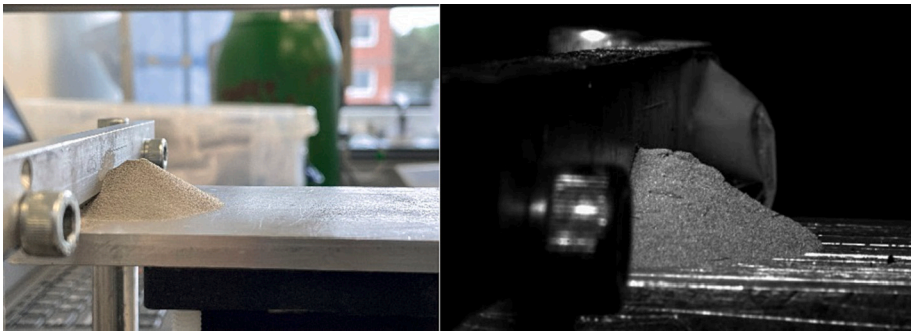

Fig. 18. Powder heap in front of blade.

powder spreadability. Relative density (also packing fraction) could be more related to the degree of compaction which defines how close the spread powder is to a solid material and several researchers [49] have reported correlations between RD and the manufactured part properties. One could also look at spreadability as the ability to spread a powder from a reservoir (e.g. hopper or heap) to a surface (or in a space) with the same packing sate as it was in the reservoir. In this context, the packing density generated by the spreading process should be compared against the bulk density of the powder. Therefore, the following equation, which was also suggested by Haydari [50], could be a good indicator of the spreadability of the powders and is used in this work:

$$Spreadability\ index = \frac{Bulk\ density\ of\ spread\ layer}{Bulk\ density\ of\ powder} \quad (8)$$

Fig. 19 shows the spreadability index of both GA and HDH samples on with the fixed gap size of 191 μm (slightly larger than d_{90} of both powders ensuring at least one particle layer is spread) at different blade speeds. it can be seen that the HDH powder a has lower spreadability index in comparison to the GA powder. The irregular shape of HDH powder could lead to a looser rearrangement of particles during spreading process and resulted in lessening the spreadability index. Nevertheless, both powders have not reached their bulk density values. Although most researchers do not report quantitatively acceptable values for the spreadability index (or packing fraction) after spreading, Narra et al. [41] have reported that HDH can be used in PBF, despite its low packing fraction after spreading. Furthermore, by increasing the spreading speed, the spreadability index of both powders reduces, with a drastic reduction of spreadability index for the HDH powder at 200 mm/s. This might be a result of the blade spreading mechanism which induces the dragging of irregular shape particles and could move them from one place to another over the bed surface [51,52].

Fig. 20 shows the spreadability index of GA and HDH powders after spreading using the pocket bed system. The results indicate that the HDH powder has lower spreadability index than the GA powder. The spreading speed still reduces the spreadability index of the two powders, but with a lower impact as compared to the free surface bed spreading (Fig. 19).

The results overall shows that the GA powder has a better spreadability than the HDH powder, which can be correlated with the flow measurements obtained from all the techniques. This could be due to the shape of HDH powders as it is expected that irregular particles could have less flow tendencies than the spherical particles due to the particle interlocking [53]. However, it can be seen that spreadability of both powders reduces as the spreading speed is increased, showing powder behaviour could be sensitive to the strain rate. The FT4 rheometer stability test results show that the flow energy for the HDH and GA powders increases as the blade tip speeds is decreased from 70 to 10 mm/s, suggesting that both powders have lower resistance against flow at higher blade speeds, under the downwards movement of the blades where the powder is relatively confined. This may be contrary to the results obtained from the spreading test, where the spreadability index decreases with the spreading speeds. The powder flow resistance under dynamic conditions is obviously an important parameter which is often overlooked by most powder flow studies, perhaps due to the limited technical availability. The discrepancies between the results of dynamic flow tests and the spreadability in this work can be regarded as an emphasis on the existing gap in the knowledge of dynamic powder flow and highlights the need for gaining a better understanding of the correlation between powder spreadability and powder flow, for which development of state of the art measurement techniques and modelling capabilities would be vital.

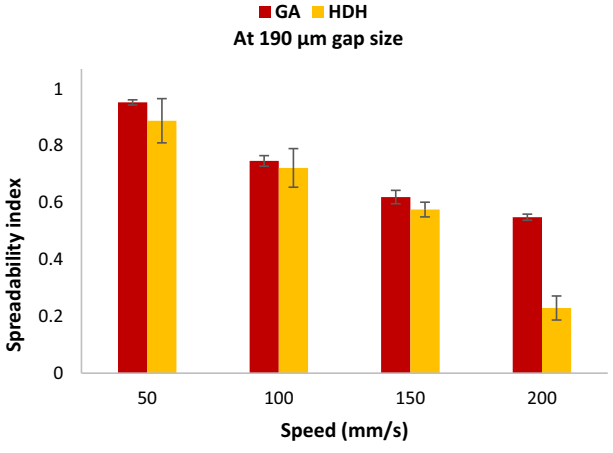

Fig. 19. Spreadability index of both powders at 191 μm gap size and different blade speeds.

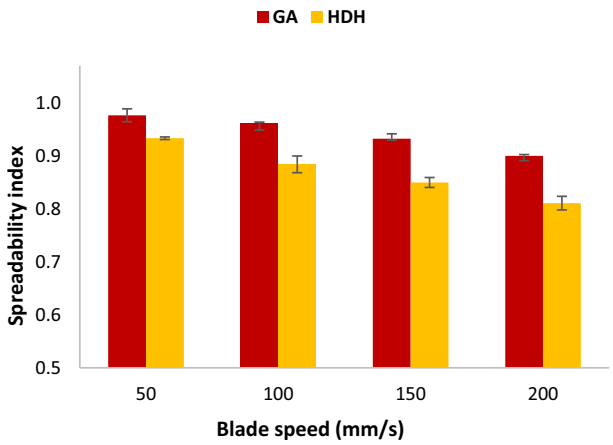

Fig. 20. Comparison of spreadability index for GA and HDH powder in one pocket (1 mm).

5. Conclusions

The purpose of this study was to characterise bulk flow properties of two different grades of Ti6Al4V metal powders, namely the GA and HDH, and to carry out an experimental characterisation of their spreading behaviour using an in-house spreading rig, in order to develop better understanding of the correlation between the flow of powders and their spreading behaviour. As part of this study, the flowability of both samples was characterised using the static and dynamic angle of repose, powder Hausner ratio and Carr index, powder flow rate through an orifice, the FT4 rheology, flow function from ring shear cell (at different consolidation stresses) and the powder hardness from ball indention test. The following conclusions could be drawn from this work:

- All techniques indicated that the two powders behave under free to easy flowing categories while the GA powder has a better flowability than the HDH powder.
- The spreading results is compared with the flow measurements obtained from all the techniques. It was found that the GA powder with higher flowability has a quantitatively higher spreadability index than the HDH powder. The irregular shape of HDH powder leads to a looser arrangement of particles and lessens the spreadability index especially at higher blade speeds.
- The spreadability index of both powders decreases as the spreading speed is increased, showing the powder behaviour could be sensitive to the strain rate.
- The flow measurement under the dynamic condition using the FT4 rheometer shows that both the HDH and GA powders have higher flow resistance under the lower blade rotation speed, which disagrees with the behaviour of powder during spreading when the blade speed is increased.

CRediT authorship contribution statement

Mozhdeh Mehrabi: Conceptualization, Methodology, Investigation, Data curation, Visualization, Formal analysis, Writing – original draft. **Jabbar Gardy:** Methodology, Data curation, Formal analysis, Investigation, Visualization, Writing – review & editing. **Fatemeh Talebi:** Investigation, Data curation, Formal analysis. **Amin Farshchi:** Investigation, Data curation, Formal analysis, Writing – review & editing. **Andrew Bayly:** Conceptualization, Methodology, Supervision, Writing

– review & editing. **Ali Hassanpour:** Supervision, Conceptualization, Methodology, Writing – review & editing.

Declaration of Competing Interest

The authors declare that they have no known competing financial interests or personal relationships that could have appeared to influence the work reported in this paper.

Data availability

Data will be made available on request.

Acknowledgment

The authors would like to acknowledge financial support from EPSRC-UK Future Manufacturing Hub in Manufacture using Advanced Powder Processes (MAPP) (EP/P006566/1, www.mapp.ac.uk). The authors would like to thank Dr Colin Hare and Dr Azza Mahmoud for the training and providing access to the low stress shear cell equipment at the University of Surrey.

References

[1] M. Attaran, The rise of 3-D printing: The advantages of additive manufacturing over traditional manufacturing, Business Horizons 60 (5) (2017) 677–688.
[2] T.S. Srivatsan, T.S. Sudarshan, Additive Manufacturing: Innovations, Advances, and Applications, CRC Press, 2015.
[3] L.E. Murr, E. Martinez, K.N. Amato, S.M. Gaytan, J. Hernandez, D.A. Ramirez, P. W. Shindo, F. Medina, R.B. Wicker, Fabrication of metal and alloy components by additive manufacturing: examples of 3D materials science, J. Mat. Res. Technol. 1 (1) (2012) 42–54.
[4] I. Campbell, O. Diegel, J. Kowen, T. Wohlers, Wohlers Report 2018: 3D Printing and Additive Manufacturing State of the Industry: Annual Worldwide Progress Report, Wohlers Associates, 2018.
[5] J.J. Lewandowski, M. Seifi, Metal additive manufacturing: a review of mechanical properties, Annu. Rev. Mater. Res. 46 (2016).
[6] Y. He, J. Gardy, A. Hassanpour, A.E. Bayly, A digital-based approach for characterising spread powder layer in additive manufacturing, Mater. Des. 196 (2020), 109102.
[7] F. Suska, G. Kjeller, P. Tarnow, E. Hryha, L. Nyborg, A. Snis, A. Palmquist, Electron beam melting manufacturing technology for individually manufactured jaw prosthesis: a case report, J. Oral Maxillofac. Surg. 74 (8) (2016) 1706–e1.
[8] E. Kaivosoja, V.M. Tiainen, Y. Takakubo, B. Rajchel, J. Sobiecki, Y.T. Konttinen, M. Takagi, Materials used for hip and knee implants, in: Wear of Orthopaedic Implants and Artificial Joints, Woodhead Publishing, 2013, pp. 178–218.
[9] Shunyu Liu, Yung C. Shin, Additive manufacturing of Ti6Al4V alloy: a review, Mater. Des. 164 (2019).
[10] Z. Liu, C. Huang, C. Gao, R. Liu, J. Chen, Z. Xiao, Characterization of Ti6Al4V powders produced by different methods for selective electron beam melting, J. Min. Metall. B: Metall. 55 (1) (2019) 121–128.
[11] G. Chen, S.Y. Zhao, P. Tan, J. Wang, C.S. Xiang, H.P. Tang, A comparative study of Ti-6Al-4V powders for additive manufacturing by gas atomization, plasma rotating electrode process and plasma atomization, Powder Technol. 333 (2018) 38–46.
[12] S. Haeri, Y. Wang, O. Ghita, J. Sun, Discrete element simulation and experimental study of powder spreading process in additive manufacturing, Powder Technol. 306 (2016) 45–54. ISSN 0032–5910.
[13] S. Vock, B. Klöden, A. Kirchner, T. Weißgärber, B. Kieback, Powders for powder bed fusion: a review, Progr. Addit. Manuf. (2019) 1–15.
[14] W. Gao, Y. Zhang, D. Ramanujan, K. Ramani, Y. Chen, C.B. Williams, C.C. Wang, Y. C. Shin, S. Zhang, P.D. Zavattieri, The status, challenges, and future of additive manufacturing in engineering, Comput. Aided Des. 69 (2015) 65–89.
[15] S. Vock, B. Klöden, A. Kirchner, T. Weißgärber, B. Kieback, Powders for powder bed fusion: a review, Progr. Addit. Manuf. (2019) 1–15.
[16] A. Simchi, The role of particle size on the laser sintering of iron powder, Metall. Mater. Trans. B Process Metall. Mater. Process. Sci. 35 (5) (2004) 937–948.
[17] Y. Shi, Z. Li, H. Sun, S. Huang, F. Zeng, Effect of the properties of the polymer materials on the quality of selective laser sintering parts, Proc. Inst. Mech. Eng. Part L J. Mat. Design Appl. 218 (3) (2004) 247–252.
[18] A.T. Sutton, C.S. Kriewall, M.C. Leu, J.W. Newkirk, Powders for additive manufacturing processes: characterization techniques and effects on part properties, Solid Freeform Fabric. 1 (2016) 1004–1030.
[19] G.P. Bierwagen, T.E. Sanders, Studies of the effects of particle size distribution on the packing efficiency of particles, Powder Technol. 10 (3) (1974) 111–119.
[20] A.C. Hoffmann, H.J. Finkers, A relation for the void fraction of randomly packed particle beds, Powder Technol. 82 (2) (1995) 197–203.
[21] J. Zheng, W.B. Carlson, J.S. Reed, The packing density of binary powder mixtures, J. Eur. Ceram. Soc. 15 (5) (1995) 479–483.
[22] N.P. Karapatis, G. Egger, P.E. Gygax, R. Glardon, Optimization of powder layer density in selective laser sintering, in: 1999 International Solid Freeform Fabrication Symposium, 1999.
[23] A.B. Spierings, G. Levy, Comparison of density of stainless steel 316L parts produced with selective laser melting using different powder grades, in: Proceedings of the Annual International Solid Freeform Fabrication Symposium, 2009, August, pp. 342–353. Austin, TX.
[24] H. Attar, K.G. Prashanth, L.C. Zhang, M. Calin, I.V. Okulov, S. Scudino, C. Yang, J. Eckert, Effect of powder particle shape on the properties of in situ Ti–TiB composite materials produced by selective laser melting, J. Mater. Sci. Technol. 31 (10) (2015) 1001–1005.
[25] D.S. Nasato, T. Pöschel, Influence of particle shape in additive manufacturing: Discrete element simulations of polyamide 11 and polyamide 12, Addit. Manuf. 36 (2020), 101421.
[26] I.E. Anderson, E.M. White, R. Dehoff, Feedstock powder processing research needs for additive manufacturing development, Curr. Opinion Solid State Mater. Sci. 22 (1) (2018) 8–15.
[27] S. Berretta, O. Ghita, K.E. Evans, A. Anderson, C. Newman, Size, shape and flow of powders for use in Selective Laser Sintering (SLS), in: High Value Manufacturing: Advanced Research in Virtual and Rapid Prototyping, 2013, p. 49.
[28] L. Markusson, Powder Characterization for Additive Manufacturing Processes, 2017.
[29] Y.Y. Sun, S. Gulizia, C.H. Oh, C. Doblin, Y.F. Yang, M. Qian, Manipulation and characterization of a novel titanium powder precursor for additive manufacturing applications, Jom 67 (3) (2015) 564–572.
[30] Y. Ma, T.M. Evans, N. Philips, N. Cunningham, Numerical simulation of the effect of fine fraction on the flowability of powders in additive manufacturing, Powder Technol. 360 (2020) 608–621.
[31] M. Mehrabi, A. Hassanpour, A. Bayly, An X-ray microtomography study of particle morphology and the packing behaviour of metal powders during filling, compaction and ball indentation processes, Powder Technol. 385 (2021) 250–263.
[32] H.H. Hausner, Friction Conditions in a Mass of Metal Powder, Polytechnic Inst. of Brooklyn. Univ. of California, Los Angeles, 1967.
[33] R.L. Carr, Evaluating flow properties of solids, Chem. Eng. 18 (1965) 163–168.
[34] A. Zocca, C.M. Gomes, T. Mühler, J. Günster, Powder-bed stabilization for powder-based additive manufacturing, Adv. Mechan. Eng. 6 (2014), 491581.
[35] D. Geldart, E.C. Abdullah, A. Hassanpour, L.C. Nwoke, I.J.C.P. Wouters, Characterization of powder flowability using measurement of angle of repose, China Particuol. 4 (03n04) (2006) 104–107.
[36] D. Schulze, Flow Properties of Powders and Bulk Solids. 2006–2011, 2022.
[37] B.H. Kaye, J. Gratton-Liimatainen, N. Faddis, Studying the avalanching behaviour of a powder in a rotating disc, Part. Part. Syst. Charact. 12 (5) (1995) 232–236.
[38] H. Gu, H. Gong, J.J.S. Dilip, D. Pal, Effects of powder variation on the microstructure and tensile strength of Ti6Al4V parts fabricated by selective laser melting, in: 2014 International Solid Freeform Fabrication Symposium, University of Texas at Austin, 2014.
[39] R. Freeman, Measuring the flow properties of consolidated, conditioned and aerated powders—a comparative study using a powder rheometer and a rotational shear cell, Powder Technol. 174 (1–2) (2007) 25–33.
[40] J. Clayton, Optimising metal powders for additive manufacturing, Metal Powd. Rep. 69 (5) (2014) 14–17.
[41] S.P. Narra, Z. Wu, R. Patel, J. Capone, M. Paliwal, J. Beuth, A. Rollett, Use of non-spherical hydride-dehydride (HDH) powder in powder bed fusion additive manufacturing, Addit. Manuf. 34 (2020), 101188.
[42] P. Mellin, O. Lyckfeldt, P. Harlin, H. Brodin, H. Blom, A. Strondl, Evaluating flowability of additive manufacturing powders, using the Gustavsson flow meter, Metal Powd. Rep. 72 (5) (2017) 322–326.
[43] D. Schulze, Powders and Bulk Solids: Behaviour, Characterization, Storage and Flow, 1st edition, Springer, Germany, 2007.
[44] Y. Tan, J. Zhang, X. Li, Y. Xu, C.Y. Wu, Comprehensive evaluation of powder flowability for additive manufacturing using principal component analysis, Powder Technol. 393 (2021) 154–164.
[45] A. Hassanpour, M. Ghadiri, Characterisation of flowability of loosely compacted cohesive powders by indentation, Part. Part. Syst. Charact. 24 (2) (2007) 117–123.
[46] U. Zafar, C. Hare, A. Hassanpour, M. Ghadiri, Ball indentation on powder beds for assessing powder flowability: Analysis of operation window, Powder Technol. 310 (2017) 300–306.
[47] Y. Yan, E. Chibowski, A. Szcześ, Surface properties of Ti-6Al-4V alloy part I: Surface roughness and apparent surface free energy, Mater. Sci. Eng. C 70 (2017) 207–215.
[48] L. Cordova, T. Bor, M. de Smit, M. Campos, T. Tinga, Measuring the spreadability of pre-treated and moisturized powders for laser powder bed fusion, Addit. Manuf. 32 (2020), 101082.
[49] C.A. Chatham, T.E. Long, C.B. Williams, A review of the process physics and material screening methods for polymer powder bed fusion additive manufacturing, Prog. Polym. Sci. 93 (2019) 68–95.
[50] Z. Haydari, The Spreading Behaviour of Stainless Steel Powders for Additive Manufacturing, Doctoral dissertation, University of Leeds, 2021.
[51] Q. Li, V. Rudolph, B. Weigl, A. Earl, Interparticle van der Waals force in powder flowability and compactibility, Int. J. Pharm. 280 (1–2) (2004) 77–93.
[52] D. Ruggi, C. Barrès, J.Y. Charmeau, R. Fulchiron, D. Barletta, M. Poletto, A quantitative approach to assess high temperature flow properties of a PA 12 powder for laser sintering, Addit. Manuf. 33 (2020) 101143.
[53] Z. Wu, M. Asherloo, R. Jiang, M.H. Delpazir, N. Sivakumar, M. Paliwal, J. Capone, B. Gould, A. Rollett, A. Mostafaei, Study of printability and porosity formation in

laser powder bed fusion built hydride-dehydride (HDH) Ti-6Al-4V, Addit. Manuf. 47 (2021) 102323.